Noname manuscript No.
(will be inserted by the editor)

Coverage Maximization with Autonomous Agents in Fast Flow Environments

Andrew Kwok · **Sonia Martínez**

Communicated by Emilio Frazzoli

Abstract **This work examines the cooperative motion of a group of autonomous vehicles in a fast flow environment. The magnitude of the flow velocity is assumed to be greater than the available actuation to each agent. Collectively, the agents wish to maximize total coverage area defined as the set of points reachable by any agent within T time. The reachable set of an agent in a fast flow is characterized using optimal control techniques. Specifically, this work addresses the complementary cases where the static flow field is smooth, and where the flow field is piecewise constant. The latter case arises as a proposed approximation of a smooth flow that remains analytically tractable. Furthermore, the techniques used in the piecewise constant flow case enable treatment for obstacles in the environment. In both cases, a gradient ascent method is derived to maximize the total coverage area in a distributed fashion. Simulations show that such a network is able to maximize the coverage area in a fast flow.**

Keywords Optimal Sensor Coverage · Distributed Control of Multi-agent Systems

Mathematics Subject Classification (2000) MSC 93C99 · MSC 49J15

1 Introduction

The development of novel schemes that allow for the re-adaptation of unmanned vehicles to changing environmental conditions is a vigorously studied field [1–3]. Indeed, the pervasiveness of miniaturized embedded devices has spurred a great interest in the production of lower-cost autonomous vehicles. However, the low power capacity of these vehicles can severely affect the system autonomy and performance. This may be the case when operating in harsh environments, where the actuation of a vehicle may not be sufficient to deal with

Work supported by grants NSF CAREER Award CMMI-0643679 and NSF CNS-0930946.

A. Kwok
Opera Solutions, San Diego

S. Martínez
Mechanical and Aerospace Engineering, 9500 Gilman Drive, La Jolla, CA 92093
E-mail: soniamd@ucsd.edu

environmental disturbances. In this work, we consider the case where the environment prevents an agent from maintaining a constant position, or even revisiting previous locations. Such scenarios are motivated by applications, such as performing surveillance or monitoring operations with lightweight UAVs in a large storm system. Specifically, we will assume that the agents move in an *a priori* known flow field, but the field is faster than the absolute maximum speed of an agent. We wish to enable a group of cooperative vehicles to move such that the area of the reachable set of points in the flow environment is maximized.

Contributions. The main contribution of this work is an algorithmic solution to the autonomous deployment of vehicles to maximize coverage in a fast flow environment. This can be used as a high-level routine for the deployment of UAVs in cooperative surveillance or sensing tasks. We encode this objective through a performance metric that the agents wish to maximize as the total area of all points reachable within a chosen time horizon T. This metric contains global information since it is the sum of all the individual vehicles' reachable areas. However, using gradient ascent techniques, we show that local maximization is possible with knowledge of only a subset of other agent locations.

We restrict our study to flows that are either affine or piecewise constant, which allows us to provide an analytical characterization of the gradient ascent direction that vehicles must follow. Additionally, we allow for the presence of obstacles in the piecewise constant flow case. The notion of reachable sets motivates the study of time-optimal trajectories within these two respective flow fields. Hence, we characterize the behavior of time-optimal trajectories for each flow case. While there is a rich body of existing literature regarding motion planning with and without obstacles in various environments, we provide results that are specifically adapted to the problem that we are addressing. In particular, we study the different cases of time-optimal trajectories that may arise in a piecewise constant flows, and use these cases as a basis of a gradient-based coverage motion algorithm.

Literature review. The problem of path planning in a flow field has its roots in the classical optimal control problem known as Zermelo's navigation problem [4], whose solution relies on use of the Pontryagin minimum principle, as in [5]. Motion planning for single vehicles in a flow has been lately studied [6, 7]. More recently, [8–10] characterizes the optimal trajectories for a Dubins-like vehicle in the presence of constant flows, while [11] presents a robust control strategy for a Dubins' vehicle in non-constant flows. The paper [12] provides a generalization of time-optimal course changes for a Dubins vehicle moving across a heterogeneous terrain, and across boundaries where the vehicle dynamics change.

A rich body of literature exists for obstacle avoidance, such as [13–16]. The approach that we take in this work most resembles the results found in [13–15], where different possible cases of minimum-time trajectories are considered and characterized. In particular, [14, 15] deal with the scenario where the environment exhibits piecewise constant regions with differing trasversal costs, which results in a type of Snell's law for trajectories. However, the resulting behavior of time-optimal trajectories is different from the results we present here for fast flows. Namely, with hilly terrain as in [14] one finds that having "switchback" type paths may be time-optimal, while in the flow environment we consider, only straight paths are feasible. In [15], the authors examine the case where refracted trajectories may move along interfaces between regions; similar to the results described in this paper, except that in [15], the piecewise constant regions are isotropic with respect to desired travel direction.

Regarding cooperative motion of multiple vehicles in a flow environment, the authors in [17] have demonstrated stable formation control in the presence of an external time-invariant flow field. However, that work assumes that individual vehicles have full controllability. Similarly, [18] addresses the case of maintaining a stable formation for sampling in an

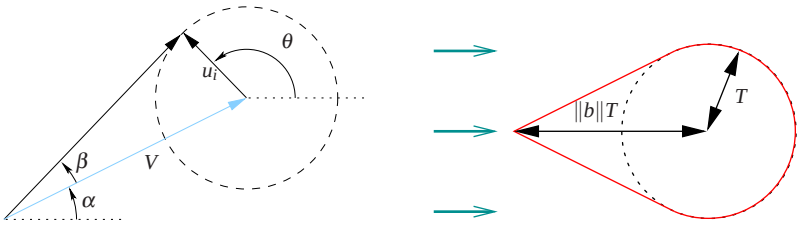

Fig. 1 On the left, illustration of the β, and α quantities. The dashed circle represents the set of inputs u_i with magnitude 1. On the right, the reachable set $\mathscr{R}_T(p_{i0})$ for p_{i0} under a constant horizontal flow.

ocean environment with exogenous currents, while [19] combines time-optimal trajectories in a constant flow field with formation stabilization.

With the exception of [9] and [20], previous work has considered the motion control problem of vehicles in a slow flow. That is, the vehicles had sufficient actuation to move against the flow. We utilize a simple kinematic model, as in [17], to consider flows which are both spatially varying and fast. Furthermore, much previous work, such as [9], consider constant flow fields. In the interest of obtaining analytic solutions, we consider piecewise constant flow fields as an approximation of smooth spatially varying flows, such as in [20]. Such a consideration introduces several interesting effects regarding time-optimal trajectories over discontinuous flows. The work of [12] considers a similar situation, except that the effect of the environment only imposes a change in maximum velocity of a vehicle. This is not the case for this work due to the directionality of flows in the environment.

2 Problem Statements and Definitions

We consider the following kinematic model:

$$\dot{p}_i = u_i + V(p_i), \tag{1}$$

where $u_i(t)$ and $V(p_i)$ are piecewise smooth, $\|u_i\| \leq 1$, and $\|V\| > 1$, and the drift $V(p_i)$ models an environmental flow field. Because of this, an agent cannot maintain a constant position, and is always pushed along the flow.

Definition 2.1 (Reachable set) *The* reachable set, $\mathscr{R}(p_{i0})$, *of an agent at position p_{i0} is the set of points $x \in X$ that an agent can reach in finite time starting from p_{i0} and using a piecewise smooth control input $u_i(t)$ with $\|u_i\| \leq 1$. The T-*limited reachable set, $\mathscr{R}_T(p_{i0})$, *of an agent at position p_{i0}, is the set of points that an agent can reach within time T using a piecewise smooth control input $u_i(t)$ with $\|u_i\| \leq 1$.*

The definition of the T-limited reachable set motivates the study of time-optimal trajectories in Sections 3–5. It can be shown, see [5], page 77, that maximum actuation is a necessary condition for time optimality. Thus, for time optimal trajectory calculations, we assume that $u_i = (\cos\theta_i, \sin\theta_i)^\mathsf{T}$.

To better relate flow field and agent motion, we utilize the following two parameters to describe the flow field. Referencing Figure 1, first $\alpha(x) = \text{atan2}(V_2(x), V_1(x))$, is the flow direction. Next, $\beta : X \to]0, \frac{\pi}{2}[$ denotes the maximum feasible angle away from $\alpha(x)$ that the agent can move in. More precisely, given $V(x)$ and $\|u_i\| = 1$, the endpoint of an agent's velocity vector (1) lies on the dashed circle of Figure 1. Using trigonometry, one can

show that $\beta(x) = \arcsin\left(\frac{1}{\|V(x)\|}\right)$. Additionally, the choice of headings θ that result in these maximal travel directions are $\theta = \alpha(x) \pm (\beta(x) + \frac{\pi}{2})$. The feasible set of directions that an agent at p_i would be able to travel in is then the interval $[\alpha(p_i) - \beta(p_i), \alpha(p_i) + \beta(p_i)]$.

Problem 1 Our main objective will be to define a distributed algorithm for the deployment of agents in a flow environment. Specifically, we wish to maximize the area coverage metric:

$$\mathscr{H}(p_1, \ldots, p_n) := \int_{\bigcup_{i=1}^n \mathscr{R}_T(p_i)} 1 dx. \tag{2}$$

This must be done without the need for all-to-all inter-agent communication, and it must take into account the flow environment's influence on agent dynamics.

We will employ a gradient ascent approach to maximize $\mathscr{H}$, since this technique lends itself easily to distributed implementation. One can imagine that, as an agent i moves in a general flow environment, the shape of $\mathscr{R}_T(p_i)$ can change in complicated ways. However, knowledge of how this change works is crucial in a gradient approach, as we would like to pick the direction of motion for each agent that results in the greatest gain of reachable area. Let ∂Y denote the boundary of a set $Y \subseteq X$. A key observation for this problem is that, for a fixed T, points along $\partial\mathscr{R}_T(p_i)$ correspond to endpoints of time optimal trajectories. The choice of T is constrained by inter-vehicle communication restrictions (see Section 6).

Therefore, to address Problem 1, we will need to study the nature of time optimal trajectories in a flow environment. We will examine two distinct but complementary problems. The first flow environment will be the affine flow field. For this case, we will use the following set of assumptions.

Assumption A1 *The coverage domain X is simply connected, convex, bounded, and the vector field V describing the flow is:*

1. *time invariant and affine in x, $V(x) = Ax + b$, for any $A \in \mathbb{R}^{2\times 2}$ and $b \in \mathbb{R}^2$,*
2. *$\|V(x)\| > 1$ for all $x \in X$.*

Under Assumption A1, we would like to solve the following problem.

Problem 2 Given Assumption A1, an agent with initial position $p_i(0) = p_{i0}$, and subject to dynamics (1), determine an expression for time optimal trajectories.

In Section 3, we will describe some properties of the reachable sets under Assumption A1 as well as present the solution to Problem 2.

Examining affine flow fields is quite restrictive, however consideration of general smooth flow fields results in solutions of the time optimal control problem that are, in general, unsolvable in closed form. Therefore, in the interest of tractability, we examine piecewise constant fields:

Assumption A2 *The flow environment X may have obstacles and:*

1. *the flow V is piecewise constant. That is, $X = \bigcup_{k=1}^m X_k$, such that $V_{|X_k}$ is constant and satisfies $\|V_{|X_k}\| > 1$ for all k,*
2. *the regions X_k, $k \in \{1, \ldots, m\}$, are separated by curves $\psi_k^\ell : X_k \to \mathbb{R}$, which are piecewise differentiable. More precisely, the curve defined by $\psi_k^\ell(x) = 0$ separates the flow regions k and $\ell \in \{1, \ldots, m\}$ and defines $\partial X_k \cap \partial X_\ell$,*
3. *the flow regions X_k are closed sets. Therefore, along the boundary between two neighboring regions X_k, X_ℓ, we enable the agent to flow according to either constant flow velocity.*

Under these assumptions, we will solve the problem:

Problem 3 Given Assumption A2, an agent with initial position $p_i(0) = p_{i0}$, and subject to dynamics (1), characterize the behavior of time optimal trajectories.

In Sections 4 and 5, we will heavily exploit the fact that time-optimal trajectories are simple to compute in the interior of constant flow regions. However, the discontinuity between flow regions complicates the characterization of trajectories through multiple flow regions. Furthermore, certain intersections of time optimal trajectories with flow region boundaries lead to interesting behavior, which we detail in Section 5.

3 Affine Flows

In this section, we characterize the time-optimal trajectories and reachable set of an agent in a continuously differentiable flow field. This will solve Problem 2, which will be employed to solve Problem 1. The results build on the known analysis for the Zermelo problem that we briefly present here for the sake of completeness.

By choosing u_i such that an agent is always heading $\pm\beta$ away from α, we can compute the boundary of the reachable set. Specifically, these inputs take the form

$$u_i(p_i) = \begin{bmatrix} \cos(\alpha(p_i) \pm (\beta(p_i) + \frac{\pi}{2})) \\ \sin(\alpha(p_i) \pm (\beta(p_i) + \frac{\pi}{2})) \end{bmatrix}. \tag{3}$$

We state some properties of the reachable set and refer the reader to [21] for the proofs.

Proposition 3.1 *Under Assumption A1, the extreme trajectories computed using* (3)*, which define the reachable set boundary, intersect only at the initial position p_{i0}.*

Theorem 3.1 *Under Assumption A1, the reachable set $\mathscr{R}(p_{i0})$ has no holes.*

In order to find $\mathscr{R}_T(p_{i0})$, we need to obtain all the solutions to the optimal control problem:

$$\begin{aligned} &\text{minimize:} && J = \int_0^{t_f} 1 dt\,, \\ &\text{subject to:} && \dot{p}_i = u_i + V(p_i)\,, \|u_i\| \leq 1\,, \text{given } p_i(0) \text{ and } p_i(t_f)\,, \end{aligned} \tag{4}$$

for a given time $t_f \leq T$, initial condition $p_i(0) = p_{i0}$ and free final condition $p_i(t_f)$. For a smooth flow field V, this is known as Zermelo's problem, and a solution can be found [5], page 78. The optimal solution is to consider a control input of the form $u_i = (\cos\theta_i, \sin\theta_i)^\mathsf{T}$ with

$$\dot{\theta}_i = \sin^2\theta_i \frac{\partial V_2}{\partial x_1} + \sin\theta_i \cos\theta_i \left(\frac{\partial V_1}{\partial x_1} - \frac{\partial V_2}{\partial x_2} \right) - \cos^2\theta_i \frac{\partial V_1}{\partial x_2}\,. \tag{5}$$

The minimum-time trajectories are obtained by using this input in combination with (1). Given a fixed $p_i(T)$ in the reachable set, one can find an specific optimal trajectory via a shooting method.

To define the T-limited boundary, one can integrate (1) using (5) to time T, starting at p_{i0} for various initial headings $\theta_i(0) \in [\alpha - \beta - \frac{\pi}{2}, \alpha + \beta + \frac{\pi}{2}]$. The solutions can be then recorded and combined with the extreme travel curves for $t \in [0, T]$ to give the boundary of $\mathscr{R}_T(p_{i0})$. Finally, we define $\tau\colon X \times X \to \mathbb{R}_{\geq 0} \cup \{\infty\}$ to be the minimum travel time between two points in X. The minimum travel time $\tau(x,y)$ is computed from the solution to (4) for an agent starting at x and ending at y. Due to the flow, in general, $\tau(x,y) \neq \tau(y,x)$.

Remark 3.1 Time-optimal solutions can in some situations cease to be optimal at a given point. This is known in the optimal control literature as a *conjugate point*. Roughly speaking, a conjugate point along an optimal trajectory (or geodesic), occurs wherever that geodesic intersects another geodesic. However, due to the result in [22], optimal trajectories corresponding to linear flow fields do not have conjugate points. This can be readily extended to the case of affine flows. In this way, T can be arbitrarily large without the risk of incorrectly approximating the T-limited reachable set by joining the endpoints of solutions of the Pontryagin minimum principle, (4) and (5).

Remark 3.2 The reachable set $\mathscr{R}_T(p_{i0})$ can be approximated by a discrete set of points on the boundary by choosing a subset of angles. As the number of angles to sample the reachable set increases, the approximation converges to the true reachable set. To find an accurate approximation, one can employ $\{\theta_k\}_{k=1}^N \subseteq [\alpha(p_i)-\beta(p_i)-\frac{\pi}{2}, \alpha(p_i)+\beta(p_i)+\frac{\pi}{2}] \equiv [a,b]$, with $\theta_{k+1} = a+\frac{k}{N-1}(b-a)$, $k=0,\ldots,N-1$, with N sufficiently large. However, depending on the shape of the reachable set, and how the optimal trajectories vary with θ, we may require a large N to obtain an acceptable representation. With knowledge of the curves defining the T-limited boundary of $R_T(p_i)$ (that is, the points in $R_T(p_i)$ that are reached at time T), and the two extreme optimal trajectories, one can attempt to use an adaptive sampling procedure to find better $\{\theta_k\}_{k=1}^N$. Several papers are available in the literature regarding the approximation of convex curves by a set of points [23,24]. Typically, curves are assumed to be known, piecewise convex or concave, with known inflection points; thus, the approximation problem is restricted to the convex/concave sub-pieces. For example, [25] quantifies the error of the approximation of the boundary of a convex set $Q \subseteq \mathbb{R}^2$ by a set of n points P_n defining an inner polygon, $P_n \subseteq Q$. In particular, it is proven that, as $n \to +\infty$, the approximation error is given as:

$$E \approx \frac{1}{12n^2}\int_0^{2\pi}\left(\rho(r)^{2/3}dr\right)^3 = \frac{1}{12n^3}\left(\int_\ell \kappa(\ell)^{1/3}d\ell\right)^3,$$

where $\rho(r)$ is the curvature radius of the boundary, κ its curvature, and ℓ an arc-length parameterization of the curve. The authors [25] then suggest the method of *empirical distributions* to place the points in $P_n = \{r_1,\ldots,r_n\}$ to provide an optimal approximation as $n \to +\infty$. The r_i should satisfy that $\int_{r_i}^{r_{i+1}} \rho(r)^{2/3}dr$ has equal value for all i. This means that, the higher the curvature radius, the closer the points have to be in order to represent it. The representation and sampling of $R_T(p_i)$ can be based on the method of empirical distributions (which can be extended to non-convex boundaries). If the T boundary of R_T was known, then one could choose points $p_{1f},\ldots,p_{Nf} \in R_T$ to satisfy the above criterion. Then, for each p_{kf}, one can solve the minimum-time optimal control problem to find the corresponding angle θ_k and optimal trajectory joining $p_i(0)$ with p_{kf}. These would be more adapted angles to represent R_T. Similarly, one would have to choose times $t_k \in [0,T]$, to approximate each of the optimal extreme trajectories of $R_T(p_i)$. To deal with the fact that the T-limited portion of $R_T(p_i)$ is unknown, one would have to estimate somehow the value $\rho(r)$ (or $\kappa(\ell)$) between two sampling points p_{kf}, p_{k+1f}, which could be done via a finer sampling. This idea was used in the paper [26] to approximate non-convex boundaries. Finally, as p_i moves, the boundaries will change with time. A good adaptive algorithm would take into account the variation of the optimal trajectories in a neighborhood of p_i in order to forecast if the boundaries become more curved or not. This issue requires further study for the affine and piecewise constant case in the following sections. In case the flow is constant in one direction and linear in the other it can be seen that the boundary of reachable sets are

composed of straight and circular lines. For these cases, the approximations using constant inter-angle sampling works well.

For affine flows, the dynamics (1) take the form

$$\dot{p}_i = Ap_i + b + u_i = \begin{pmatrix} a_{11} & a_{12} \\ a_{21} & a_{22} \end{pmatrix} p_i + \begin{pmatrix} b_1 + \cos\theta_i \\ b_2 + \sin\theta_i \end{pmatrix}. \tag{6}$$

The time-optimal steering input given by (5) with the affine flow parameters is

$$\dot{\theta}_i = a_{21}\sin^2\theta_i + (a_{11} - a_{22})\sin\theta_i\cos\theta_i - a_{12}\cos^2\theta_i\,.$$

Note that the above differential equation is separable, and one can obtain an explicit solution for $\theta_i(t)$ up to quadratures (possibly in implicit integral form). The system described by (6) is linear in p_i, and so the time-optimal trajectories in an affine flow are given by

$$p_i(t) = e^{At}p_i(0) + \int_0^t e^{A(t-s)}(b + u_i(s))ds\,. \tag{7}$$

For the constant flow case, $A = 0$ and $\|b\| > 1$, the set $\mathscr{R}_T(p_i)$ resembles Figure 1. The extreme travel curves are straight line segments at angles $\pm\beta$ away from the flow direction. They are joined by a circular arc with radius T centered at a distance $\|b\|T$ downstream. The set for affine flows is a deformed version of this shape.

4 Piecewise Constant Flows: Simple Trajectories

With the aim of extending algorithms to a wider family of flows, we further develop the previous results to piecewise constant flows addressing Problem 3. Thus, this section and the following one detail the various types of optimal trajectories that may occur in a piecewise constant flow.

Under Assumption A2, optimal paths in the interior of each region X_k will be straight lines since the flow in each region is constant. The last item in Assumption A2 applies mainly for the scenario where it is possible for an agent to move along the interface between two flow regions. This specific case will be handled in Section 5.

Suppose an agent begins at p_0 and heading θ_0. Then, there will be a sequence of optimal course changes corresponding to each time an agent travels into a new flow region. We enumerate these with a subscript ℓ. Furthermore, $\bar{t}_\ell$ and $\bar{x}_\ell$ will be the time and location of a trajectory's crossing from the $(\ell-1)$th region to the ℓth region, with the convention that $\bar{t}_0 = 0$ and $\bar{x}_0 = p_0$. When necessary, we denote the first and second components of $\bar{x}_\ell$ as $\bar{x}_{\ell,1}$ and $\bar{x}_{\ell,2}$, respectively.

4.1 Catalog of Optimal Trajectories

Before launching into the detailed description of each type of trajectory and how they occur, we summarize the various types of optimal trajectories we find in a piecewise constant flow. We categorize the time-optimal trajectories into two broad categories:

Definition 4.1 *A* simple trajectory *is a time optimal trajectory where each point of intersection with a flow region boundary $\bar{x}_\ell$ occurs transversely. Furthermore, this simple trajectory does not intersect any other time optimal trajectory. A trajectory that is not a simple trajectory is a* non-simple trajectory.

We note that transverse intersections with the environment boundaries, i.e. obstacles, are collisions, and the simple trajectory ends at that final intersection point. Non-simple trajectories are primarily trajectories that have a *tangential* intersection with a flow region boundary. This results in a wide range of interesting phenomena that will be investigated in Section 5. We reserve the remainder of this section to describe simple trajectories. Unless otherwise stated, the proofs of all statements can be found in the thesis [21].

4.2 Simple Trajectories

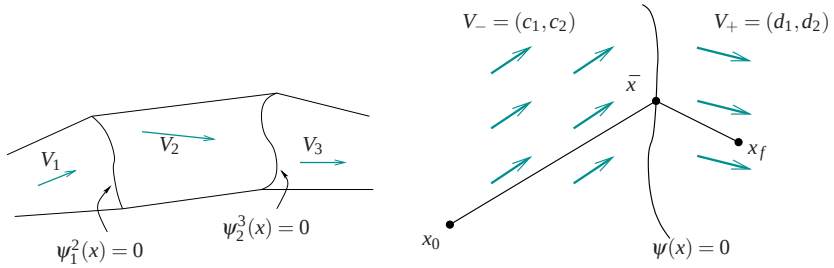

Fig. 2 On the left, a general piecewise flow case. On the right, a graphical example of the relation between incident and refracted angle of a vehicle at the interface between two regions of different constant flows.

Referencing Figure 2, consider that the vehicle begins at x_0, the interface between two regions X_1, X_2, occurs at the smooth level set of $\psi(x)=0$, and the two constant flows are given by $V_-=(c_1,c_2)^\mathsf{T}$ and $V_+=(d_1,d_2)^\mathsf{T}$.

The following proposition determines the heading change that an optimal trajectory will undergo when transitioning from X_1 to X_2:

Proposition 4.1 *Let $V_-=(c_1,c_2)^\mathsf{T}$ and $V_+=(d_1,d_2)^\mathsf{T}$ be the flows in two neighboring regions, and α_1, α_2 be their respective flow orientations. Let ξ be the orientation of the normal vector of the smooth curve $\psi(x)=0$ at the point where the optimal trajectory crosses into the second flow region. Let θ_- and θ_+ be the control inputs of the optimal trajectories inside regions X_1 and X_2, respectively. A necessary condition for an optimal trajectory across the interface of the two flow regions requires that:*

$$\frac{1+\|V_-\|\cos(\theta_- -\alpha_1)}{\sin(\theta_- -\xi)}=\frac{1+\|V_+\|\cos(\theta_+ -\alpha_2)}{\sin(\theta_+ -\xi)}. \tag{8}$$

Given (8)*, and a fixed heading θ_-, the final heading satisfies*

$$\sin\theta_+=\frac{B\pm C\sqrt{B^2+C^2-1}}{B^2+C^2}, \tag{9}$$

with $B=\dfrac{1+\|V_-\|\cos(\theta_- -\alpha_1)}{\sin(\theta_- -\xi)}\cos\xi-d_2\,,\ C=\dfrac{1+\|V_-\|\cos(\theta_- -\alpha_1)}{\sin(\theta_- -\xi)}\sin\xi+d_1.$

Remark 4.1 For certain choices of initial headings θ_-, the system of equations in the proof of Proposition 4.1 may have no solution. These special angles correspond to the choice of extreme headings $\theta_-=\alpha_1\pm\left(\beta_1+\frac{\pi}{2}\right)$. However, the solution of θ_+ as a function of θ_- has

a well-defined limit as $\theta_- \to \alpha_1 \pm \left(\beta_1 + \frac{\pi}{2}\right)$. Additionally, it may be that there is no solution for θ_+ in (9). This may occur when $B^2 + C^2 - 1 < 0$. However, since (9) is a necessary condition for optimality, the fact that there is no real-valued θ_+ satisfying (9) implies that there is no optimal continuation of a particular trajectory that intersects the boundary between two flows; see Figure 5 for an example. Trajectories following flow interfaces or encountering obstacles will be studied in Section 5.

5 Piecewise Constant Flows: Non-simple Trajectories

We now study how consideration of flow boundaries, obstacles, or boundaries between two neighboring flow regions affects the optimal trajectories. We refer to these optimal trajectories as *non-simple trajectories.*

5.1 Obstacles

By obstacles in the flow, we refer to holes in the flow environment and boundaries marking impassable regions, such as in Figure 3. Such phenomena may impede a simple trajectory.

Before introducing the next lemma, we define $*$, the path concatenation operator. Given two parameterized paths $\rho_1, \rho_2 \colon [0,1] \to \mathbb{R}^2$, such that $\rho_1(1) = \rho_2(0)$, the concatenation of the two paths, $\rho = \rho_1 * \rho_2$ is such that $\rho(0) = \rho_1(0)$ and $\rho(1) = \rho_2(1)$.

Lemma 5.1 *Let ρ be a feasible trajectory in a constant flow environment without obstacles from $\rho_0 = \rho(0)$ to $\rho_f = \rho(1)$. Choose $s_1, s_2 \in [0,1]$ with $s_1 < s_2$ and let ρ_1 be the section of $\rho(s)$ for $0 \le s < s_1$ and ρ_2 be the section of $\rho(s)$ for $s_2 \le s \le 1$. Let the function J take a parameterized path ρ and return the time required to trasverse it in the constant flow. Suppose μ is the straight line path from $\rho(s_1)$ to $\rho(s_2)$. Then, $\tilde{\rho} = \rho_1 * \mu * \rho_2$ has the property that $J(\tilde{\rho}) \le J(\rho)$.*

In other words, by replacing a section of a trajectory with a straight line path, the time to trasverse that path is shortened. Next, we consider the situation when an optimal trajectory intersects an obstacle (or flow environment boundary).

Definition 5.1 *Let ζ be a parameterized curve in the flow environment. Then, ζ is* locally convex *at $\zeta(\bar{s})$ relative to the flow domain X if there exists a $\delta > 0$ such that, for every $s \in]\bar{s} - \delta, \bar{s} + \delta[$, $s \neq \bar{s}$, and for all $t \in [0,1]$, we have $\zeta(\bar{s}) + t(\zeta(s) - \zeta(\bar{s})) \in X$. Similarly, ζ is* locally concave *at $\zeta(\bar{s})$ relative to X if there exists a $\delta > 0$ such that, for $s \in]\bar{s} - \delta, \bar{s} + \delta[$, $s \neq \bar{s}$, and for all $t \in [0,1]$, $\zeta(\bar{s}) + t(\zeta(s) - \zeta(\bar{s})) \notin X$.*

The convex (resp. concave) curve ζ is strictly convex *(resp.* strictly concave*) if there exists $\delta > 0$, such that, for all $t \in [0,1]$, $\zeta(\bar{s}) + t(\zeta(s) - \zeta(\bar{s})) \neq \zeta(\tilde{s})$ for all $\tilde{s} \in]\bar{s} - \delta, \bar{s} + \delta[$.*

With these definitions we can state the following result regarding non-simple paths.

Theorem 5.1 *Let ζ be a parameterization of the boundary of an obstacle. If ζ is locally strictly concave at the point $\zeta(s)$, then time-optimal trajectories that are tangent at $\zeta(s)$ may result in non-simple paths. These paths are formed by following the boundary ζ, and then tangentially leaving as a straight line path into the interior of X.*

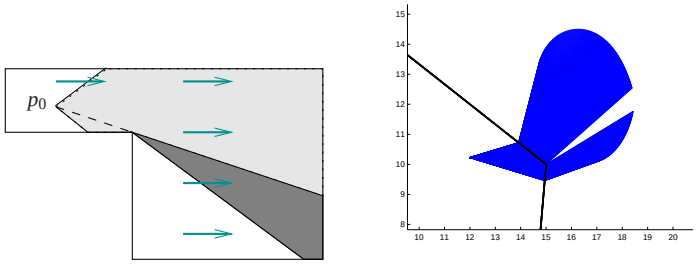

Fig. 3 On the left, the light-gray area is the subset of $R(p_0)$ that can be reached by following simple trajectories. Non-simple trajectories are obtained going from p_0 to the corner in the environment and continuining with a straight line in the dark-grey area. On the right, a scenario where simple trajectories form a gap

Remark 5.1 Cases where ∂X is not smooth can be seen as a limiting case of Theorem 5.1. Similarly, non-smooth points along $\partial X_k - \partial X \cap \partial X_k^c$ can be seen as a limiting case of Proposition 4.1. Both scenarios are illustrated in Figure 3. Here, the set of points reachable by simple trajectories is shaded light gray, while the non-simply reachable points are shaded as dark gray. Time optimal trajectories to reach the occluded region must follow the black dashed line, and then change course at the corner.

Definition 5.2 *We define a* course change *to be either a discontinuous change in heading as described in* (8) *or the sequence of navigating around an obstacle described in Theorem 5.1.*

5.2 Intersecting Trajectories

Multiple simple or non-simple trajectories may intersect in two possible ways. The first instance involves trajectories that intersect at the same time, and the second instance involves trajectories that intersect at different times. In both cases, the individual trajectories are optimal up until the point where they intersect. Then, a decision must be made to determine which trajectory (if any) to continue based on travel time. Such scenarios highlight the

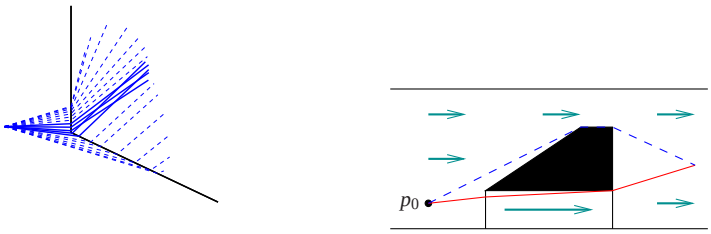

Fig. 4 On the left, a scenario where simple trajectories intersect each other. On the right, a path flows around an obstacle faster than the other. The dashed path terminates at the intersection.

fact that the Pontryagin minimum principle along with the Bellman principle of optimality are necessary conditions. Thus, while a particular trajectory $\rho_1(t)$, originating from p_0 and passing through $x \in X$, may satisfy Proposition 4.1 and Theorem 5.1, it does not imply that

$\rho_1(t)$ is the only trajectory satisfying those results that passes through x. The following result formalizes the decision-making process that occurs when two time optimal trajectories intersect.

Proposition 5.1 *Let $\rho_1(t)$ and $\rho_2(t)$ be two distinct time optimal trajectories originating from p_0. Suppose that there exist $t_1 > 0$ and $t_2 > 0$ such that $\rho_1(t_1) = \rho_2(t_2)$, and that this is the first intersection between ρ_1 and ρ_2. In other words, $t_1 = \min_t\{\rho_1(t) = \rho_2(s) \mid s > 0\}$. Then,*

1. *if $t_1 < t_2$, then $\rho_1(t)$ is time optimal for $t \in [0, t_1]$,*
2. *if $t_1 = t_2$, then the optimality of both trajectories is restricted to only points in $\rho_1(t)$, $\rho_2(t)$ for $t \in [0, t_1]$,*
3. *if $t_1 > t_2$, then $\rho_1(t)$ is time optimal for $t \in [0, t_1[$.*

The first and third cases of Proposition 5.1 involve simple trajectories that intersect at different times. This can occur with flow around an obstacle, as in Figure 4. It may be that flow on one side of the obstacle is faster or shorter. Then it is possible for a trajectory that takes the faster path to intersect a trajectory that travels the slower path. Intersecting trajectories can also occur when an agent travels along a flow interface as in Figure 5. Upon crossing a flow interface, the new course change may result in an agent that travels along the interface. Then, some trajectories are blocked by the trajectory flowing along the interface.

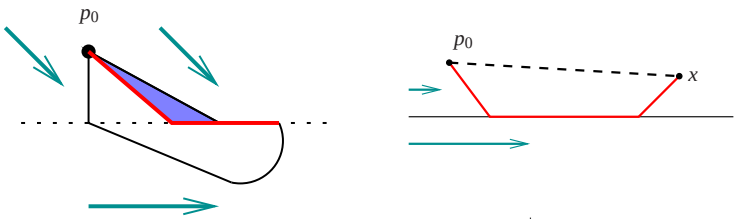

Fig. 5 On the left, a scenario where simple trajectories starting at p_0 trasverse through the shaded region terminate at the flow interface (dotted line). There is a non-simple trajectory (thick red line) that flows along the interface after switching into the lower region. The black line is the boundary of the reachable set. On the right, a scenario where it may be faster to follow the solid path to reach a final destination, x, rather than a simple trajectory (dotted line). This is due to the faster flow velocity in the bottom region.

The second case of Proposition 5.1 introduces the case of simple trajectories intersecting at the same time. This may occur when there is a flow interface that is convex relative to the incoming flow as in Figure 4.

5.3 Trajectories Along Flow Interfaces

The flow case shown in Figure 5 motivates additional study of trajectories that flow along the interface of two constant regions. Application of (8) can result in a trajectory that travels along the boundary between two different flows. Use of the same result can also give a way to compute a heading back into the first region. This leads to trajectories, as in Figure 5.

We now show that the existence of an initial heading θ_- that results in an outgoing trajectory that is tangent with the flow interface. For simplicity, suppose we have a two-region flow with parameters $\alpha_1 = \alpha_2 = 0$, $1 < \|V_-\| < \|V_+\|$, $\xi = \frac{\pi}{2}$. This corresponds to the

cartoon shown in Figure 5. We seek a solution to θ_- in (8) that results in $\theta_+ = 0$. This implies that the trajectory, after switching, moves along the flow interface. A few computations lead to $\cos\theta_- = \dfrac{1}{1+\|V_+\|-\|V_-\|}$. Note here that the assumption that $\|V_+\| > \|V_-\|$ is important in order to have a well-defined solution.

Now we wish to solve the subsequent question. Once we are flowing along the boundary in the faster flow region, what is the optimal heading change back into the slower region? To find this out, consider $\alpha_1 = \alpha_2 = 0$, $1 < \|V_+\| < \|V_-\|$, $\xi = \dfrac{\pi}{2}$. Setting $\theta_- = 0$ and solving for θ_+ from (8) leads to $\cos\theta_+ = \dfrac{1}{1+\|V_-\|-\|V_+\|}$. Again, since $\|V_-\| > \|V_+\|$, the solution for θ_+ is well-defined.

Although we have considered a simple example for how a trajectory can flow along a boundary, this may happen for other choices of α_1, α_2. When an agent is moving along a flow boundary, and it is possible to switch back into the first region, the agent may choose to switch back at any time, making this process indeterminate. However, the result above dictates that there is only one possible outgoing heading back into the first flow region.

The following result summarizes the above analysis for general flow parameters, which we omit in this manuscript; see [21] for a proof.

Proposition 5.2 *Assume that two flow regions, defined by $\|V_-\|, \alpha_1$ and $\|V_+\|, \alpha_2$, respectively, are separated by an interface whose normal angle is ξ. If it is possible for an agent to flow along the boundary under the second flow, then θ_+ satisfies*

$$\theta_+ = \xi + \pi \pm \arccos\left[\|V_+\|\sin\left(\xi + \frac{\pi}{2} - \alpha_2\right)\right]. \tag{10}$$

Let $D = \dfrac{1+\|V_+\|\cos(\theta_+ - \alpha_2)}{\sin(\theta_+ - \xi)}$. Then, the incoming heading resulting in flow along the boundary, if it exists, satisfies

$$\theta_- = \arctan\left(\frac{D\cos\xi - \|V_-\|\sin\alpha_1}{-D\sin\xi - \|V_-\|\cos\alpha_1}\right) \pm \arccos\left(\frac{1}{\sqrt{(D\cos\xi - V\sin\alpha_1)^2 + (D\sin\xi + \|V_-\|\cos\alpha_1)^2}}\right). \tag{11}$$

Another example of flow along interfaces can occur for the converse case where the trajectory originates from a region of faster flow, and encounters a region of slower flow as in Figure 6. While there may exist a simple trajectory that connects two points in the flow, it may be faster if the region of slow flow can be avoided. In this case, the slower region may be treated as an obstacle in the flow, and a candidate trajectory may be formed using previous techniques. Then, apply the result of Proposition 5.1 to resolve the conflict of multiple trajectories meeting at the same point. Note that, with respect to the fast flow only, the heavy red path in Figure 6 still satisfies the necessary condition of optimality described in Theorem 5.1.

5.4 Nested Non-simple Trajectories

In the previous subsections, we described scenarios where either the reachable set is larger than the set of all simple trajectories, or where simple trajectories intersect. In the case where

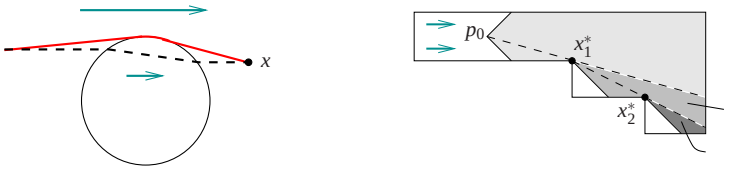

Fig. 6 On the left, a scenario showing that it may be faster to follow the solid-type of path than the dotted-like one. This is because the flow is much faster outside of the circular region. On the right, a scenario where there is a nested non-simply reachable set of points (dark gray) that cannot be reached by a simple trajectory from the corner marked x_1^*.

there is a set $\mathscr{U}(p_0)$ that is unreachable by simple trajectories as in Figure 3, it is possible to have nested non-simply reachable sets. This occurs, as in Figure 6. For such scenarios, self-similarity provides a solution for an optimal path from p_0 to a point within the non-simply reachable set.

For example, in Figure 6, we can view the problem of reaching a point in the region $\mathscr{U}_2(p_0)$ in minimum time as a minimum time problem starting from the point x_1^*. By repeatedly applying the result from the previous subsection, an optimal path from p_0 to a point in $\mathscr{U}_2(p_0)$ can be obtained. By the principle of optimality, this path is correct since all sub-paths are optimal trajectories.

Remark 5.2 This notion of self-similarity provides a systematic method of constructing an approximation of the reachable set of points for piecewise constant flow fields (in the presence of obstacles). Because of the nature of fast flows, the time optimal set of headings to choose from falls within the interval $\theta \in [\alpha-(\beta+\frac{\pi}{2}),\alpha+(\beta+\frac{\pi}{2})]$. At each instance where a optimal trajectory undergoes a course change due to an obstacle, one can re-sample a new set of trajectories with initial headings in the range of feasible headings. For example, suppose that R_0 is the set of trajectories from p_i to an obstacle polygon P_0. For every vertex of P_0, v, consider the set of intersection-free trajectories that can be reached from v, say R_v. Then, one can update $R_1 = R_0 \cup R_v$. The complexity of computing a reachable set when an obstacle is present in the flow should not be larger than the complexity of computing it when it goes across several arbitrary region configurations. In fact, an obstacle can be considered as a flow of "0-magnitude" surrounded by an "∞-magnitude" flow. Additionally, one could leverage the fact that optimal trajectories emanating from the obstacle in the known environment are known and can be computed off-line in order to simplify the reachable-set calculations. The complexity of representing and computing reachable sets can be high when T is large compared to region sizes or the geometry of regions/flows is complicated.

6 Area Coverage

In this section, we make use of the analysis of the previous sections and present coverage algorithms that aim to solve Problem 1 for affine and piecewise-constant flows.

Definition 6.1 *Agents i and j are* reachable set neighbors *if $\mathscr{R}_T(p_{i0}) \cap \mathscr{R}_T(p_{j0} \neq \emptyset$. Thus, agent i is trivially a neighbor of itself. Additionally, the* neighbor set *of i, is*

$$\mathscr{N}_{i,reach} := \{j \in \{1,\ldots,n\} \mid \mathscr{R}_T(p_{i0}) \cap \mathscr{R}_T(p_{j0}) \neq \emptyset\}.$$

The reachable set graph, *$\mathscr{G}_{reach} = (V,E)$, describes the interconnection between agents in the flow environment. For $V = \{1,\ldots,n\}$, and $i,j \in V$, $(i,j) \in E$ if and only if $j \in \mathscr{N}_{i,reach}$ and vice-versa.*

The algorithms that we will develop are distributed over the reachable set graph $\mathscr{G}_{\text{reach}}$. That is, in order to properly execute the deployment process and attempt to maximize reachable area, an individual agent i only needs to communicate information with its neighbors $j \in \mathscr{N}_{i,\text{reach}}$.

Information within distance $r > 0$ is enough for each vehicle to find the set $\mathscr{N}_{i,\text{reach}}$, when $R_T(p_i) \cap R_T(p_j) \neq \emptyset$, only if $d(p_i, p_j) \leq r$. Assuming that there exist a finite upper bound for the flow magnitudes, $V_{\max} = \max_{k\in\{1,\dots,m\}} \|V_{|X_k}\| < +\infty$, the reachable sets will be definitely bounded, so there exists a finite r for which this is true. An upper bound of this range for the specific situation when the environment can be decomposed, as in Figure 2, can be found to be $r = 2T(V_{\max}+1)$. In this case, the region X consists of a finite sequence of "consecutive" regions X_i, $i \in \{1,\dots,m\}$, where only simple trajectories are possible. To see this, consider first the case of two consecutive regions X_1 followed by X_2: If $p_0 \in X_2$, then, due to the specific shape of the reachable set, as in Figure 1, the length of an optimal trajectory is always upper bounded by $\ell \leq T(V_2+1) \leq T(V_{\max}+1)$. If $p_0 \in X_1 - X_1 \cap X_2$, then a trajectory can be decomposed into two parts with lengths ℓ_1 and ℓ_2. It can be verified that $\ell_1 \leq T_1(V_{\max}+1)$, where T_1 is the time that takes the trajectory to intersect $X_1 \cap X_2$, and that $\ell_2 \leq (T-T_1)(V_{\max}+1)$. In this way, $\ell_1 + \ell_2 \leq T(V_{\max}+1)$. The T-reachable points will be then contained in a disk $D(p_0, T(V_{\max}+1))$. An induction argument can be used to guarantee that $R_T(p_0) \subseteq D(p_0, T(V_{\max}+1))$ when the reachable set crosses several regions. In general, the required r depends on the shape of the reachable set.

6.1 Gradient-based Coverage Control Algorithm

Since the goal is to maximize $\mathscr{H}$, we begin by taking the gradient of $\mathscr{H}$ with respect to p_i in order to obtain a set directions each agent must travel in.

Proposition 6.1 *Given the area objective* (2)*, let*

$$\mathscr{A}_i := \partial\mathscr{R}_T(p_{i0}) \cap \left(\bigcup_{\substack{j\in\mathscr{N}_{i,reach} \\ j\neq i}} \text{interior}(\mathscr{R}_T(p_{j0})) \right)^{\mathsf{c}} \cap X\,, \tag{12}$$

be the set of points in $\partial\mathscr{R}_T(p_{i0})$ not in the interior of neighboring reachable sets. Then the gradient with respect to p_i is:

$$\frac{\partial\mathscr{H}}{\partial p_i} := \int_{\mathscr{A}_i} \hat{\mathbf{n}}^{\mathsf{T}}(\zeta_i)\frac{\partial\zeta_i}{\partial p_i}d\zeta_i\,, \tag{13}$$

where $\zeta_i : \mathbb{S} \to \mathbb{R}^2$ is a parameterization of $\partial\mathscr{R}_T(p_{i0})$, and $\hat{\mathbf{n}} : \mathbb{R}^2 \to \mathbb{R}^2$ is the unit outward-pointing normal vector at ζ_i.

We refer the reader to [27] for the full proof of this fact. The general strategy now is to follow the gradient direction in order to maximize coverage area. We begin by examining the time-evolution of the objective function $\mathscr{H}$.

Proposition 6.2 *The rate of area increase is* locally *maximized if agents implement*

$$u_i = \begin{cases} \dfrac{\frac{\partial\mathscr{H}}{\partial p_i}}{\left\|\frac{\partial\mathscr{H}}{\partial p_i}\right\|}, & \text{if } \left\|\dfrac{\partial\mathscr{H}}{\partial p_i}\right\| \geq 1, \\ \dfrac{\partial\mathscr{H}}{\partial p_i}, & \text{if } \left\|\frac{\partial\mathscr{H}}{\partial p_i}\right\| \leq 1. \end{cases} \tag{14}$$

Depending on the direction of the gradient $\frac{\partial \mathscr{H}}{\partial p_i}$, an individual agent may not be able to maximize its own area covered. This is because $\|u_i\| = 1 < \|V\|$, so it cannot be guaranteed that each quantity in the sum can be positive due to the term $\frac{\partial \mathscr{H}}{\partial p_i} V$. Nevertheless, we can still choose u_i such that the quantity $\frac{\partial \mathscr{H}}{\partial p_i}(u_i + V)$ is maximized for all i. The next result considers a limit situation that guarantees the local maximization of the area function in an infinite, rectangular domain where the flow tends to a constant ; that is, $V(p) \to v$ for $\|p\| \to +\infty$.

Proposition 6.3 *Let X be an unbounded flow domain with parallel horizontal boundaries (an infinitely long strip). Suppose that V is a piecewise continuous flow for which we have that $[\alpha(p_i) - \beta(p_i), \alpha(p_i) + \beta(p_i)] \subseteq [-\gamma, \gamma]$, for some $0 < \gamma < \frac{\pi}{2}$, and suppose further that $V(p_i) = v(p_i) + g(p_i)$ with $\lim_{\|p_i\| \to +\infty} g(p_i) = 0$ and v a horizontal constant vector with $\|v\| > 1$. Then, the agents positions tend to the set of local maximizers of $\mathscr{H}$ under the control law* (14)*.*

Remark 6.1 One can view the above result as a type of time-varying function optimization result, where the cost eventually converges to some static value. The validity of the result for general V will occur when the area of the reachable set of a point p under $\dot{p} = V(p)$ is conserved or increased. This is a type of non-contractible flow that includes constant flows.On the other hand, by relaxing the condition $\|u_i\| < \|V\|$ to $\|u_i\| = \|V\|$, one can modify the gradient algorithm to prevent minimization of the area function by allowing agents remain static when this happens.

6.2 Computation of the Gradient of the Area Function

In general, the gradient is difficult to analytically compute due to the $\frac{\partial \zeta_i}{\partial p_i}$ term inside the integral. This term is a 2×2 matrix that represents the variation of a point along $\partial \mathscr{R}_T(p_{i0})$ as the agent position p_i varies. An analytical result would require an explicit solution to (1) using (5). However, there are certain cases where such a solution is possible.

Proposition 6.4 *Under Assumption A1,*

$$\frac{\partial \zeta_i}{\partial p_i} = e^{A\tau(p_i, \zeta_i)}. \tag{15}$$

In particular, if $A = 0$ in (15), the gradient according to (13), becomes

$$\frac{\partial \mathscr{H}}{\partial p_i} = \int_{\mathscr{A}_i} \hat{\mathbf{n}}^{\mathsf{T}}(\zeta_i) d\zeta_i. \tag{16}$$

In the piecewise constant case, the gradient expression for $\mathscr{H}$ with respect to agent positions p_i is identical to the result for continuously differentiable flows in (13); the main difference lies in the term $\frac{\partial \zeta_i}{\partial p_i}$. First, we present a result dealing with simple trajectories, and then modify it to include non-simple trajectories.

We seek a formula for the position of a trajectory at terminal time T with an initial heading θ_0 at $t = 0$, and passing through a total of $q+1$ flow regions. Thus, there will be q optimal course changes. Once the initial heading θ_0 is chosen, the sequence of optimal headings to follow, $\{\theta_1, \ldots, \theta_q\}$, within each region, can be solved along with the sequence of crossing locations, $\{\bar{x_1}, \ldots, \bar{x_q}\}$. The times of interface crossings can be expressed via the following recursive relationship:

$$\bar{t_\ell} = \bar{t}_{\ell-1} + \frac{\|\bar{x}_\ell - \bar{x}_{\ell-1}\|}{\|\dot{p}_{\ell-1}\|}.$$

Similar to the affine flow case, points on the boundary $\partial\mathscr{A}_i$ can be viewed as endpoints of simple trajectories starting at p_0. Suppose that a simple trajectory passes through a total of $q+1$ flow regions. We can express the final position at time T for this trajectory in a recursive fashion. For example, the final position at time T is given by

$$p_T = \bar{x}_q + (T - \bar{t}_q)\dot{p}_q\,. \tag{17}$$

From (17), given some arbitrary initial heading, we compute $\frac{\partial \zeta_i}{\partial p_i}$ with the following results.

Proposition 6.5 *Under Assumption A2, let $\bar{x}_0 = p_0$ and*

$$D_\ell = \left(\frac{\partial \bar{x}_\ell}{\partial \bar{x}_{\ell-1}}\right)\left(\frac{\partial \bar{x}_{\ell-1}}{\partial \bar{x}_{\ell-2}}\right)\cdots\left(\frac{\partial \bar{x}_1}{\partial \bar{x}_0}\right).$$

The derivative of (17)*, the endpoint of a simple trajectory, with respect to an initial position p_0 is*

$$\frac{\partial p_T}{\partial p_0} = D_q - \dot{p}_q \sum_{\ell=1}^{q} \frac{\partial \bar{t}_\ell}{\partial \bar{x}_{\ell-1}} D_{\ell-1}\,. \tag{18}$$

We now detail how to compute each term in (18).

Proposition 6.6 *Let an interface crossing position and time be $\bar{x}$ and $\bar{t}$, suppose that there is only one such crossing, and that the interface is differentiable at $\bar{x}$. Let $\eta = (\cos\xi, \sin\xi)^\mathsf{T}$ be the unit normal vector to the interface at $\bar{x}$. Then, for a fixed choice of heading $\dot{p}$, the Jacobian of the crossing position with respect to change in initial position is given by*

$$\frac{\partial \bar{x}}{\partial p_0} = I_2 - \frac{\left(\dot{p}\eta^\mathsf{T}\right)}{\dot{p}^\mathsf{T}\eta}\,, \tag{19}$$

where I_2 is the identity matrix of dimension 2. The Jacobian of the crossing time with respect to change in initial position is given by

$$\frac{\partial \bar{t}}{\partial p_0} = -\frac{\eta^\mathsf{T}}{\dot{p}^\mathsf{T}\eta}\,. \tag{20}$$

For non-simple trajectories, the expression for the derivative of the endpoint with respect to the initial position still follows from (18) by treating non-simple course changes, as one of the $\bar{x}_\ell$ in (18). However, the expressions (19) and (20) do not apply for course changes around obstacles or through flow interfaces that are not differentiable. We present the following result to address these cases.

Proposition 6.7 *Let p_T be the endpoint of a non-simple trajectory that undergoes q course changes. Let $\ell^* \in \{1,\ldots,q\}$ denote the* first *non-simple course change described in Theorem 5.1 or the Remark 5.1. Then, the Jacobian of the endpoint position with respect to initial position is*

$$\frac{\partial p_T}{\partial p_0} = -\dot{p}_q \sum_{\ell=1}^{\ell^*} \frac{\partial \bar{t}_\ell}{\partial \bar{x}_{\ell-1}} D_{\ell-1}\,, \tag{21}$$

with

$$\frac{\partial \bar{t}_{\ell^*}}{\partial \bar{x}_{\ell^*-1}} = \frac{1}{\|\dot{p}_{\ell^*-1}\|}\frac{(\bar{x}_{\ell^*-1} - \bar{x}_{\ell^*})^\mathsf{T}}{\|\bar{x}_{\ell^*} - \bar{x}_{\ell^*-1}\|}\,. \tag{22}$$

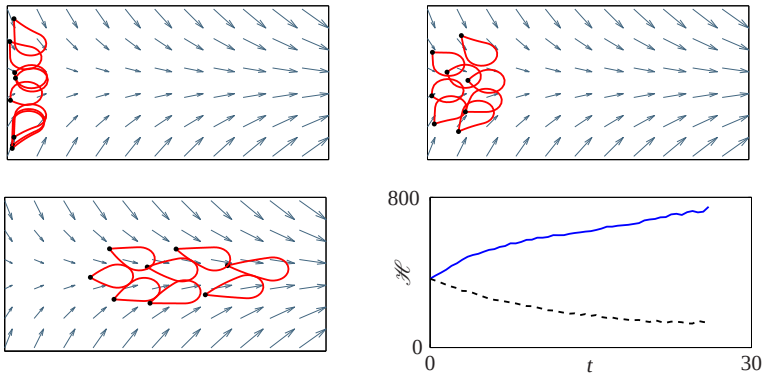

Fig. 7 Different snapshots of the area deployment algorithm in a flow for 8 agents. Times for the three snapshots are $t = 0s$ (top right), $t = 5s$ (top left), and $t = 26s$ (bottom right). Afterward, the agents leave the flow environment. A plot of the objective function is shown in the bottom graph (solid line) and a plot of the objective function for $u_i = 0$ for all i is shown in the dashed line for comparison.

The computation of $\frac{\partial \zeta_i}{\partial p_i}$ can be done approximately by using a linear interpolation of $\mathscr{R}_T(p_i)$ which uses a set of end-points $p_{1f}, \ldots, p_{Nf}$ in the T boundary of $\mathscr{R}_T(p_i)$. The variation of the linear interpolation can be expressed in terms of the variation of the end points.

Remark 6.2 The only impediment of extending the previous results to affine flows comes from the necessity of analytically computing the term $\frac{\partial \bar{t}}{\partial \bar{x}}$. An expression for $\bar{t}_\ell$ in terms of $\bar{t}_{\ell-1}$, $\bar{x}_\ell$, and $\bar{x}_{\ell-1}$, as in the proofs of Propositions 6.5 and 6.7, cannot be easily stated.

7 Simulations

The following simulation portrays a typical execution of the area coverage algorithm for the set of special flow cases described in Section 3. Here, 8 agents begin in a flow environment of length $100m$ and width $50m$. We demonstrate a case with flow parameters $a_1 1 = 0.025s^{-1}$, $b_1 = 1m/s$, $a_2 2 = -0.1s^{-1}$, and $b_2 = 0$. The simulation results are shown in Figure 7.

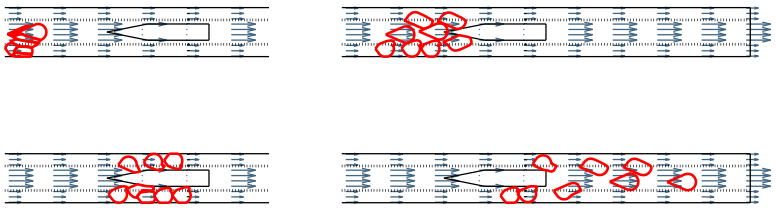

Fig. 8 Deployment in a flow environment with an island obstacle by 8 agents. The flow is also faster in the middle strip than in the regions close to the top and bottom boundaries. Simulation times from top to bottom are: $t = 0s$, $t = 10s$, $t = 20s$ and $t = 40s$.

In the next simulation, we demonstrate a piecewise constant flow domain with an obstacle. The flow environment features three parallel strips with the middle strip having a faster flow. Additionally, the obstacle is located in the middle flow region. Figure 8 gives three four snapshots of the coverage maximization as time progresses. The agents successfully navigate around the obstacle and move away from each other in order to maximize area covered. Figure 9 provides a plot of the total area covered as a function of time. One can imagine

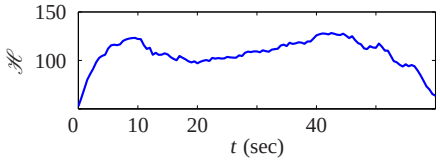

Fig. 9 Area function in the flow environment with an island.

a situation where various temperature, pressure, and other meteorological data need to be collected. This next simulation depicts 8 UAVs deploying in a hurricane-like storm system, Figure 10. The storm is modeled as a 6-sector, radially symmetric flow field. The magnitude of the central flow is 4 times an agent's airspeed in the absence of flow, while the middle and outer layers are 3.25 and 2.5 times the agent's airspeed, respectively.

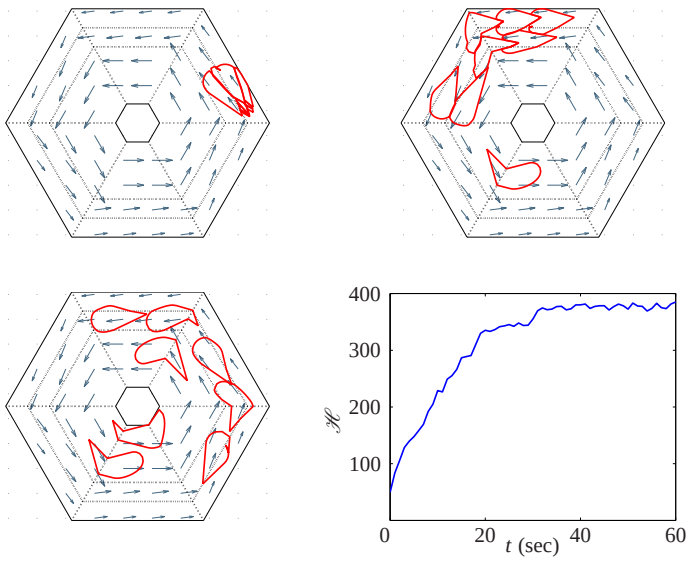

Fig. 10 The central "eye" of the storm is treated as an obstacle, or equivalently, a "no-fly zone." The simulation snapshots occur for $t = 0$ (top left), $t = 20s$ (top right), and $t = 60$ (bottom left). A plot of the total reachable area is shown in the bottom right.

8 Concluding Remarks

We addressed the problem of area coverage maximization for agents moving in a fast flow environment. The inability to move against the flow presented many interesting challenges, and we limited the set of flow environments to affine and piecewise-constant flow fields that allow us to obtain some analytical results. Possible directions of future work include consideration of alternative objective functions other than the total reachable area and the extension to other types of flows. For example, a vector field $V(x) = A(x)x + b(x)$, with $x \in X$, where $A(x) = A_0 + \varepsilon A_1(x) + \varepsilon^2 A_2(x) + \dots$ and $b(x) = b_0 + \varepsilon b_1(x) + \varepsilon^2 b_2(x) \dots$, with $A_i(x), b_i(x) \in O(\varepsilon)$, are small perturbations to constants A_0, b_0, may allow the extension of the results.

The presentation of the T-limited reachable sets involved the study of time-optimal trajectories in the respective flow environments. This allowed us to compute optimal directions of motion for the vehicles to locally maximize the group performance metric. Simulations show that, when agents are not transitioning between regions of different flow velocities, the total reachable area is maximized. This is in accord with the results derived in Section 6. However, in general, we cannot guarantee maximization of reachable area during transition from one flow region to the next. In fact, one can propose several flow environments that result in net loss of reachable area as agents deploy over the environment. In some instances, it is possible to see that the reachable-set area value fluctuates slightly around some constant value. For example, when the attracting region is made up of a finite number of flow-constant subregions, with a large size in comparison with reachable-set regions, this seems always to be the case. One can argue that, except for isolated time intervals corresponding to region changes, the vehicles reconfigure to provide relatively equal area. However, the specific value around which the area value oscillates and the amplitude of this oscillation depends very much on the parameter T and the region configuration. A relevant question to investigate is the effect of the time horizon parameter T on the algorithm performance.

The algorithm requires full knowledge of the underlying flow in order to come up with accurate approximations by piecewise constant regions. In this case, the computational effort to determine the reachable sets is justified. Otherwise, the algorithm can be used in the final stages of a flow field estimation process, when the uncertainty about the field is low.

References

1. Cortés, J., Martínez, S., Bullo, F.: Spatially-distributed coverage optimization and control with limited-range interactions. ESAIM: Control Optim. Calc. Var. 11, 691–719 (2005)
2. Hussein, I.I., Stipanovič, D.M.: Effective coverage control for mobile sensor networks with guaranteed collision avoidance. IEEE Trans. Control Syst. Technol. 15, 642–657 (2007)
3. Schwager, M., Rus, D., Slotine, J.: Decentralized, adaptive coverage control for networked robots. Int. J. Rob. Res. 28, 357 – 375 (2009)
4. Zermelo, E.: Über das navigationproble bei ruhender oder veranderlicher windverteilung. Z. Angrew. Math. und. Mech 11 (1931)
5. Bryson, A.E., Ho, Y.: Applied Optimal Control. Hemisphere Publishing Corporation, New York (1969)
6. Reif, J., Sun, Z.: Movement planning in the presence of flows. Algorithmica 39, 127–153 (2004)
7. Ceccarelli, N., Enright, J., Frazzoli, E., Rasmussen, S., Schumacher, C.: Micro UAV path planning for reconnaissance in wind. In American Control Conference, pp. 5310–5315, New York City, New York, USA (2007)
8. McGee, T.G., Spry, S., Hendrick, J.K.: Optimal path planning in a constant wind with a bounded turning rate. In AIAA Guidance, Navigation, and Control Conference and Exhibit, pp. 1–11, (2005)
9. Rysdyk, R.: Course and heading changes in significant wind. AIAA J. Gui. Control Dynam. 30, 1168–1171 (2007)

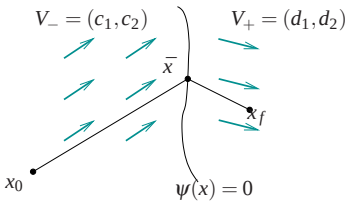

Fig. 11 Deriving the relation between incident and refracted angle of a vehicle at the interface between two regions of different, but constant, flows.

.

10. Techy, L., Woolsey, C.A.: Minimum-time path planning for unmanned aerial vehicles in steady uniform winds. AIAA J. Gui. Control Dynam. 32, 1736–1746 (2009)
11. McGee, T.G., Hendrick, J.K.: Path planning and control for multiple point surveillance by an unmanned aircraft in wind. In American Control Conference, pp. 4261–4266, Minneapolis, Minnesota, USA (2006)
12. Sanfelice, R.G., Frazzoli, E.: On the optimality of Dubins paths across heterogeneous terrain. In Hybrid systems: Computation and Control, pp. 457–470, St. Louis, Missouri, USA (2008)
13. Lozano-Perez, T., Wesley, M.: An algorithm for planning collision-free paths among polyhedral obstacles. Commun. ACM 22, 560–570 (1979)
14. Rowe, N., Ross, R.: Optimal grid-free path planning across arbitrarily contoured terrain with anisotropic friction and gravity effects. IEEE Trans. Rob. 6, 540–553 (1990)
15. Rowe, N., Alexander, R.: Finding optimal-path maps for path planning across weighted regions. Int. J. Rob. Res. 19, 83–95 (2000)
16. LaValle, S.M.: Planning Algorithms. Cambridge University Press, New York (2006)
17. Paley, D.A., Peterson, C.: Stabilization of collective motion in a time-invariant flowfield. AIAA J. Gui. Control Dynam. 32, 771–779 (2009)
18. Leonard, N.E., Paley, D., Lekien, F., Sepulchre, R., Fratantoni, D.M., Davis, R.: Collective motion, sensor networks and ocean sampling. Proc. IEEE 95, 48–74 (2007)
19. Techy, L., Smale, D., Woolsey, C.: Coordinated aerobiological sampling of a plant pathogen in the lower atmosphere using two autonomous Unmanned Aerial Vehicles. J. Field Rob. 27, 335–343 (2010)
20. Bakolas, E., Tsiotras, P.: Minimum-time paths for a small aircraft in the presence of regionally-varying strong winds. In AIAA Infotech@Aerospace, pp. 2010–3380, Atlanta, GA (2010)
21. Kwok, A.: Deployment algorithms for mobile robots under dynamic constraints. Ph.D. Thesis, University of California, San Diego (2011)
22. Serres, U.: On the curvature of two-dimensional optimal control systems and Zermelo's navigation problem. J. Math. Sci. 135, 3224–3243 (2006)
23. Gruber, P.M.: Approximation of convex bodies. In P.M. Gruber, J.M. Wills (eds.): Convexity and its Applications, pp. 131–162. Birkhauser Verlag, Boston (1983)
24. Chen, L.: Mesh smoothing schemes based on optimal Delaunay triangulations. In 13th International Meshing Roundtable, pp. 109–120, Sandia National Laboratories (2004)
25. McLure, D.E., Vitale, R.A.: Polygonal approximation of plane convex bodies. J. Math. Anal. Appl. 51, 326–358 (1975)
26. Susca, S., Martínez, S., Bullo, F.: Monitoring environmental boundaries with a robotic sensor network. IEEE Trans. Control Syst. Technol. 16, 288–296 (2008)
27. Kwok, A., Martínez, S.: A coverage algorithm for drifters in a river environment. In 2010 American Control Conference, pp. 6436–6441, Baltimore, MD, USA (2010)

A Proofs of Theorems and Propositions

Proof, Proposition 4.1. We wish to solve for the minimum-time trajectory from x_0 to a point x_f after crossing the interface between the two flows at some point $\bar{x}$. For minimum time problems, the cost function will be:

$$J = \int_0^{t_f} 1 dt = t_f \,.$$

The vehicle has dynamics $\dot{x} = F_-(x,\theta)$ or $\dot{x} = F_+(x,\theta)$ depending on which side of the flow interface it is on, where:

$$F_-(x_1,x_2,\theta) = \begin{pmatrix}\cos\theta + c_1\\ \sin\theta + c_2\end{pmatrix}, \quad \text{if } x \in X_1,$$
$$F_+(x_1,x_2,\theta) = \begin{pmatrix}\cos\theta + d_1\\ \sin\theta + d_2\end{pmatrix}, \quad \text{if } x \in X_2\,.$$

We also have the interior point boundary condition that for some time $0 < \bar{t} < t_f$, $\psi(x(\bar{t})) = 0$. One can now define the Hamiltonians for each set of dynamics as:

$$H_1(x,\theta,\lambda) = 1 + \lambda_1(\cos\theta + c_1) + \lambda_2(\sin\theta + c_2)\,,$$
$$H_2(x,\theta,\lambda) = 1 + \lambda_1(\cos\theta + d_1) + \lambda_2(\sin\theta + d_2)\,,$$

where $\lambda = (\lambda_1,\lambda_2)^\mathsf{T}$ is the costate vector. The interior boundary condition can be viewed as an additional constraint occurring at time $\bar{t}$. In this way, we adjoin the interior point constraint to the costate and Hamiltonian with a Lagrange multiplier $\nu \in \mathbb{R}$. Let $\bar{t}_-$ and $\bar{t}_+$ denote the time immediately before and after $\bar{t}$, respectively. Then,

$$\lambda^\mathsf{T}(\bar{t}_-) = \lambda^\mathsf{T}(\bar{t}_+) + \nu\frac{\partial\psi}{\partial x}\,,$$
$$H_1(x(\bar{t}_-),\theta(\bar{t}_-),\lambda(\bar{t}_-)) = H_2(x(\bar{t}_+),\theta(\bar{t}_+),\lambda(\bar{t}_+)) + \nu\frac{\partial\psi}{\partial t}.$$

We have $H_1(x(\bar{t}_-),\theta(\bar{t}_-),\lambda(\bar{t}_-)) = H_2(x(\bar{t}_+),\theta(\bar{t}_+),\lambda(\bar{t}_+))$, because there is no time dependence in ψ. Furthermore, for minimum-time optimal control problems with time-invariant dynamics, the Hamiltonian is constant and equal to zero [5], page 78. The costate jump at $\bar{t}$ is described by

$$\lambda_1(\bar{t}_-) = \lambda_1(\bar{t}_+) + \nu\frac{\partial\psi}{\partial x_1}\,, \qquad \lambda_2(\bar{t}_-) = \lambda_2(\bar{t}_+) + \nu\frac{\partial\psi}{\partial x_2}\,.$$

Using optimality with respect to the control input θ, we derive an additional set of relations:

$$\frac{\partial H_1}{\partial\theta} = -\lambda_1(\bar{t}_-)\sin\theta_- + \lambda_2(\bar{t}_-)\cos\theta_- = 0 \quad \Rightarrow \tan\theta_- = \frac{\lambda_2(\bar{t}_-)}{\lambda_1(\bar{t}_-)}\,,$$

And, similarly, $\tan\theta_+ = \dfrac{\lambda_2(\bar{t}_+)}{\lambda_1(\bar{t}_+)}$. This leads to the following six equations:

$$\begin{aligned}
&1 + \lambda_1(\bar{t}_-)(\cos\theta_- + c_1) + \lambda_2(\bar{t}_-)(\sin\theta_- + c_2) = 0\,,\\
&1 + \lambda_1(\bar{t}_+)(\cos\theta_+ + d_1) + \lambda_2(\bar{t}_+)(\sin\theta_+ + d_2) = 0\,,\\
&\lambda_1(\bar{t}_-) = \lambda_1(\bar{t}_+) + \nu\frac{\partial\psi}{\partial x_1}\,,\\
&\lambda_2(\bar{t}_-) = \lambda_2(\bar{t}_+) + \nu\frac{\partial\psi}{\partial x_2}\,,\\
&\tan\theta_- = \frac{\lambda_2(\bar{t}_-)}{\lambda_1(\bar{t}_-)}\,,\\
&\tan\theta_+ = \frac{\lambda_2(\bar{t}_+)}{\lambda_1(\bar{t}_+)}\,,
\end{aligned}$$

with the six unknowns: ν, θ_+, $\lambda_1(\bar{t}_-)$, $\lambda_2(\bar{t}_-)$, $\lambda_1(\bar{t}_+)$, and $\lambda_2(\bar{t}_+)$. Eliminating all but θ_+, we obtain:

$$\begin{aligned}
&\left(\frac{\partial\psi}{\partial x_1}\tan\theta_+ - \frac{\partial\psi}{\partial x_2}\right)(1 + c_1\cos\theta_- + c_2\sin\theta_-)\sec\theta_-\\
&= -\left(\frac{\partial\psi}{\partial x_2} - \frac{\partial\psi}{\partial x_1}\tan\theta_-\right)(1 + d_1\cos\theta_+ + d_2\sin\theta_+)\sec\theta_+\,.
\end{aligned}$$

Substitute $(c_1,c_2) = (\|V_-\|\cos\alpha_1, \|V_-\|\sin\alpha_1)$ and $(d_1,d_2) = (\|V_+\|\cos\alpha_2, \|V_+\|\sin\alpha_2)$. The relation becomes

$$\frac{1+\|V_-\|\cos(\theta_- - \alpha_1)}{\frac{\partial\psi}{\partial x_2}\cos\theta_- - \frac{\partial\psi}{\partial x_1}\sin\theta_-} = -\frac{1+\|V_+\|\cos(\theta_+ - \alpha_2)}{\frac{\partial\psi}{\partial x_1}\sin\theta_+ - \frac{\partial\psi}{\partial x_2}\cos\theta_+}\,.$$

Let ξ be the angle of the gradient vector $\nabla\psi$. That is, $\xi = \arctan\left(\frac{\frac{\partial\psi}{\partial x_2}}{\frac{\partial\psi}{\partial x_1}}\right)$. This direction is normal to the level set $\psi(x_1,x_2) = 0$. Then, the substitution $\left(\frac{\partial\psi}{\partial x_1}, \frac{\partial\psi}{\partial x_2}\right) = (\|\nabla\psi\|\cos\xi, \|\nabla\psi\|\sin\xi)$, leads to (8).

The cosine functions in the numerators of (8) can be expanded. Then, performing the substitution, $\cos\theta_+ = \sqrt{1-\sin^2\theta_+}$ yields the equation

$$(A^2+B^2)\sin^2\theta_+ + 2A\sin\theta_+ + 1 - B^2 = 0\,.$$

This is quadratic in $\sin\theta_+$, which results in (9).

Proof, Lemma 5.1. Since there are no obstacles, the point $\rho(s_2)$ is reachable from $\rho(s_1)$ via a straight line. Finally, straight line paths in a constant flow environment are time-optimal, so by replacing the middle section of ρ with a straight line segment in $\tilde{\rho}$, we have decreased the travel time along $\tilde{\rho}$ compared to ρ.

Proof, Theorem 5.1. Let ρ be a time-optimal trajectory originating from p_0 that is tangent to ζ at $\zeta(s)$. We note that, if a time-optimal trajectory intersects ζ transversely, then that trajectory must stop. First, we show that ζ must be locally concave about the intersection point $\zeta(s)$ in order to admit non-simple paths. Then, for the case when ζ is locally concave at $\zeta(s)$, we will construct non-simple (optimal) paths.

Suppose that ζ is locally strictly convex at $\zeta(s)$ and that ρ is tangent to ζ at $\zeta(s)$. The time-optimal trajectory ρ must be feasible, thus it must remain in X at all times. For ρ to continue past $\zeta(s)$, it must continue to follow the curve ζ or return into the interior of the flow region. Following the boundary is not optimal since ζ is locally convex, so there exists a neighborhood N about $\zeta(s)$ such that there is a straight line path joining $\zeta(s)$ to another point along ζ through the interior of X that also lies in N; see Figure 12. If ζ is locally convex but not strictly convex about $\zeta(s)$, then ζ is a straight line through $\zeta(s)$. Thus, straight line trajectories may continue, and ρ remains a simple trajectory.

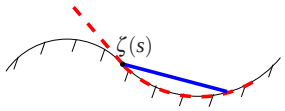

Fig. 12 Convex boundary counterexample. The thick dashed path that follows the boundary of the obstacle is not time-optimal since there exists a straight line path from $\zeta(s)$ to any point along the convex boundary, resulting in a faster time-of-arrival.

For the case that ζ is locally strictly concave at $\zeta(s)$, then the boundary of the obstacle occludes a portion of the flow domain X. Non-simple trajectories may result after this tangential intersection if it is feasible to steer along the path ζ under the constant flow. Let N be a small neighborhood about the tangential intersection point $\zeta(s)$. We first show that a trajectory that follows the boundary ζ is time-optimal. Then we combine this with the fact that, within the interior of X, time-optimal paths must be straight lines in order to complete the construction of these optimal non-simple trajectories.

Consider a trajectory ρ that connects $\zeta(s_1)$ to $\zeta(s_2)$ on the boundary of a locally strictly concave curve ζ. Suppose ρ follows the boundary ζ, but is not time-optimal. Then there exists a trajectory ρ^* connecting $\zeta(s_1)$ and $\zeta(s_2)$ with a shorter travel time. Furthermore, ρ^* must leave the boundary ζ at some point and then re-enter it in order to finish at $\zeta(s_2)$. However, since ζ is locally strictly concave, such a maneuver requires a course change within the interior of the flow region, which implies that ρ^* is not time-optimal; see Figure 13. At any point along the boundary, the time-optimal trajectory ρ may depart tangentially. This continuation of the time-optimal path satisfies Bellman's necessary principle for optimality. Furthermore, it is the only path that does so. Suppose that at some point $\zeta(s^*) \in N$, $s^* > s$, the departing trajectory is not tangential. Then it either transversely crosses ζ, which is not feasible, or it exits back into the flow domain X. Let μ be this non-tangential line. Since ζ is locally concave in N, for some small $\varepsilon > 0$, there is a straight line path from an earlier point along the boundary, $\zeta(s^* - \varepsilon)$ that necessarily intersects this non-tangential departing line, see Figure 14. By Lemma 5.1, the tangentially departing path results in a faster arrival time to the intersection point.

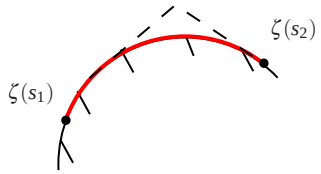

Fig. 13 A diagram demonstrating optimality of a path the follows the boundary of an obstacle. Since ζ is locally strictly concave, any other path connecting $\zeta(s_1)$ to $\zeta(s_2)$ must undergo a path change within the interior of a flow region (i.e. the dotted line). This violates the optimality condition that straight-line paths within the interior of a flow region are time-optimal.

Fig. 14 At left, an example of a non-simple (time-optimal) path around an obstacle. At right, we provide a counterexample showing that a tangentially departing path is optimal.

Proof, Proposition 5.1. Under the assumptions of the Proposition, ρ_1 and ρ_2 are time optimal up until the intersection point. By time optimality, the trajectory that reaches the intersection point $\rho_1(t_1) = \rho_2(t_2)$ first is the fastest trajectory to that point. This addresses the cases where the intersection times are not equal.

Suppose instead that $\rho_1(t_1) = \rho_2(t_2) \triangleq x$, with $t_1 = t_2$ and x inside the interior of a region X_k. Suppose that ρ_1 continues to be the time-optimal path to go from p_0 to $y = \rho_1(t)$ for $t > t_1$. Then the trajectory composed of $\rho_2(t)$ until x and $\rho_1(t)$ until y would also be time-optimal (it takes the same time to reach y from p_0). This is a contradiction with the fact that inside the region X_k, optimal trajectories must be straight lines.

Proof, Proposition 5.2 We begin by stating the useful identity

$$a\cos\theta + b\sin\theta = \sqrt{a^2+b^2}\cos(\theta-\phi)\,,$$
$$\phi = \arctan\left(\frac{b}{a}\right).$$

Given that the outgoing trajectory flows along the flow interface, we have the following condition

$$\tan\left(\xi \pm \frac{\pi}{2}\right) = \frac{\sin\left(\xi \pm \frac{\pi}{2}\right)}{\cos\left(\xi \pm \frac{\pi}{2}\right)} = \frac{\sin\theta_+ + \|V_+\|\sin\alpha_2}{\cos\theta_+ + \|V_+\|\cos\alpha_2}\,.$$

The left hand side denotes the tangent direction at the interface crossing while the right hand side denotes the resultant velocity of an agent. We now solve for the outgoing vehicle heading θ_+. Throughout we note that we keep track of the plus/minus signs so that they remain consistent.

$$\frac{\pm\cos\xi}{\mp\sin\xi} = \frac{\sin\theta_+ + \|V_+\|\sin\alpha_2}{\cos\theta_+ + \|V_+\|\cos\alpha_2},$$
$$\pm\cos\xi\cos\theta_+ \pm \|V_+\|\cos\alpha_2\cos\xi = \mp\sin\xi\sin\theta_+ \mp \|V_2\|\sin\alpha_2\sin\xi,$$
$$\cos\xi\cos\theta_+ \pm \sin\xi\sin\theta_+ = \mp\|V_+\|\sin(\alpha_2+\xi)\,.$$

At this point, we apply the trigonometric identity for addition of sin and cos.

$$\cos\left[\theta_+ - \arctan\left(\frac{\pm\sin\xi}{\pm\cos\xi}\right)\right] = \mp\|V_+\|\sin(\alpha_2+\xi),$$
$$\cos(\theta_+ \mp \xi) = \mp\|V_2\|\sin(\alpha_2+\xi)\,.$$

At this point, we take the inverse cosine of both sides. However, due to the multiplicity of solutions for arccos, we will again have two possible solutions. Before proceeding with arccos, we split the two existing solutions

we already have to obtain–in the end–four total possible solutions.

$$\begin{cases}\theta_+ - \xi = \pm\arccos[-\|V_+\|\sin(\alpha_2+\xi)]\,,\\ \theta_+ + \xi = \pm\arccos[\|V_+\|\sin(\alpha_2+\xi)]\,,\end{cases}$$

$$\begin{cases}\theta_+ = \xi \pm\arccos[-\|V_+\|\sin(\alpha_2+\xi)]\,,\\ \theta_+ = xi \pm\arccos[\|V_+\|\sin(\alpha_2+\xi)]\,.\end{cases}$$

Thus, we have achieved the first result of this proposition. Now we assume that θ_+ is known and satisfies the first result. We wish to solve for the incoming heading θ_- that achieves an outgoing heading of θ_+. To simplify some clutter, we let

$$D = \frac{1+\|V_+\|\cos(\theta_+-\alpha_2)}{\sin(\theta_+-\xi)}\,.$$

Now we solve for θ_-:

$$\begin{aligned}&\frac{1+\|V_-\|\cos(\theta_- - \alpha_1)}{\sin(\theta_- + \xi)} = D,\\ &1+\|V_-\|(\cos\theta_-\cos\alpha_1+\sin\theta_-\sin\alpha_1) = D(\sin\theta_-\cos\xi-\cos\theta_-\sin\xi),\\ &(\|V_-\cos\alpha_1+D\sin\xi)\cos\theta_- + (\|V_-\|\sin\alpha_1 - D\cos\xi)\sin\theta_- = -1.\end{aligned}$$

We apply the trigonometric identity for addition of sin and cos.

$$\sqrt{(\|V_-\|\cos\alpha_1+D\sin\xi)^2+(\|V_-\|\sin\alpha_1-D\cos\xi)^2}\cdot\cos\left(\theta_- - \arctan\left[\frac{\|V_-\|\sin\alpha_1-D\cos\xi}{\|V_-\|\cos\alpha_1+D\sin\xi}\right]\right) = -1\,.$$

Applying arccos with multiplicity of solutions in mind and solving for θ_- leads to the final result.

Proof, Proposition 6.2. We consider the time evolution of the cost function by applying the chain rule:

$$\dot{\mathscr{H}} = \sum_{i=1}^{n}\frac{\partial\mathscr{H}}{\partial p_i}\dot{p}_i = \sum_{i=1}^{n}\frac{\partial\mathscr{H}}{\partial p_i}(u_i+V)\,.$$

Each agent's contribution to the rate of change of $\mathscr{H}$ is then given by $\frac{\partial\mathscr{H}}{\partial p_i}(u_i+V) = \frac{\partial\mathscr{H}}{\partial p_i}u_i + \frac{\partial\mathscr{H}}{\partial p_i}V$. However, there is the constraint that $\|u_i\|\le 1$. The choice of u_i that maximizes each individual term of the sum is the vector that points in the same direction as $\frac{\partial\mathscr{H}}{\partial p_i}$, but with magnitude 1.

Proof, Proposition 6.3. Since $g(p)$ is piecewise continuous, for every $\varepsilon>0$ there is $r>0$ such that $\|g(p)\|\le\varepsilon$ for $\|p\|>r$. Define $\rho := \min\{\|v\|-\varepsilon, \min_{\|p\|\le r}\|V(p)\|\}$, then $\rho>1$. Consider the vector w with angle γ and norm $\rho-1>0$. From our analysis of the reachable set, we have $\dot{x}_i = V_x(p_i)+u_i^x \ge w_x$. Thus, we have $\|p_i(T+t)-p_i(t)\|\ge w_xT$ and $\|p_i(T+t)\|\ge -\|p_i(t)\|+w_xT\ge 0$ for large enough T. In other words, the flow makes $\|p_i(t)\|\to+\infty$, when p_i evolves under (14).

The vector field $V(p)$ is bounded and piecewise continuous, thus the function $f(p)=\text{area}(\mathscr{R}_T(p))$ is continuous and bounded, with $\text{area}(\mathscr{R}_T(p))\le A$. Define $0\le W(p_1,\dots,p_n) := -\mathscr{H}(p_1,\dots,p_n)+nA\le nA$, for every $p_1,\dots,p_n$. We can rewrite:

$$\dot{W} = -\sum_i\frac{\partial\mathscr{H}}{\partial p_i}(u_i+V(p_i)) = -\sum_i\frac{\partial\overline{\mathscr{H}}}{\partial p_i}(\bar{u_i}+\tilde{u}_i+v) - \frac{\partial\mathscr{H}}{\partial p_i}g(p_i) + \frac{\partial h(p_1,\dots,p_n)}{\partial p_i},$$

where $\overline{\mathscr{H}}$, (resp. $\overline{\mathscr{A}}_i$, $\bar{u_i}$), are the corresponding functions (resp. regions, control law) associated with the dynamics $\tilde{p_i}=u_i+v$, $\tilde{u}_i=u_i-\bar{u_i}$, and $h(p_1,\dots,p_n)=\int_{\cup\mathscr{R}_T(p_i)\setminus\cup\mathscr{R}_T(p_i)}dq$. Because of the assumptions on the flow, we have that $\lim_{t\to+\infty}h(p_1(t),\dots,p_n(t))=0$, $\lim_{t\to+\infty}\frac{\partial h}{\partial p_i}(t)=0$ and $\lim_{t\to+\infty}\tilde{u}_i(t)\to 0$. Further, since $\frac{\partial\mathscr{H}}{\partial p_i}(p_1,\dots,p_n)$ is bounded and $\lim_{t\to+\infty}g(p_i(t))=0$, we have $\lim_{t\to+\infty}\frac{\partial\mathscr{H}}{\partial p_i}(p_i(t))g(p_i(t))=0$.

Let us see now that $\sum_i\frac{\partial\overline{\mathscr{H}}}{\partial p_i}(u_i+v)\to c\ge 0$, with $t\to\infty$. To show this, we will prove that

$$\sum_{i=1}^{n}\int_{\overline{\mathscr{A}}_i}\hat{\mathbf{n}}^{\mathsf{T}}(\zeta_i)d\zeta_i = 0\,.$$

From the definition of $\overline{\mathscr{A}}_i$ (12)

$$\overline{\mathscr{A}}_i = \partial\overline{\mathscr{R}_T}(p_{i0}) \cap \partial\left(\bigcup_{j=1}^{n} \overline{\mathscr{R}_T}(p_{j0})\right) \cap X\,.$$

Then, note that each $\overline{\mathscr{A}}_i$ is disjoint except at the isolated points where two regions $\overline{\mathscr{R}_T}(p_{i0})$ and $\overline{\mathscr{R}_T}(p_{j0})$ meet. Furthermore, $\partial\left(\bigcup_{i=1}^{n}\overline{\mathscr{R}_T}(p_{i0})\right)\cap X = \bigcup_{i=1}^{n}\overline{\mathscr{A}}_i$.

Since $\bigcup_{i=1}^{n}\overline{\mathscr{R}_T}(p_{i0})\cap X$ is compact, then the divergence theorem states that:

$$0 = \int_{\partial\left(\bigcup_{i=1}^{n}\overline{\mathscr{R}_T}(p_{i0})\cap X\right)} n\,ds = \int_{\partial\left(\bigcup_{i=1}^{n}\overline{\mathscr{A}}_i\right)} n\,ds = \sum_{i=1}^{n}\int_{\overline{\mathscr{A}}_i} n\,ds\,.$$

In other words, $\sum_{i=1}^{n}\frac{\partial\overline{\mathscr{H}}}{\partial p_i} = 0$.

From here we have that

$$\sum_{i=1}^{n}\frac{\partial\overline{\mathscr{H}}}{\partial p_i}(\bar{u_i}+v) = \sum_{i=1}^{n}\frac{\partial\overline{\mathscr{H}}}{\partial p_i}\bar{u_i} + \frac{\partial\overline{\mathscr{H}}}{\partial p_i}v = \sum_{i=1}^{n}\frac{\partial\overline{\mathscr{H}}}{\partial p_i}\bar{u_i}\,.$$

Since v is a constant, the second term in the summation is zero. This implies that $\sum_{i=1}^{n}\frac{\partial\overline{\mathscr{H}}}{\partial p_i}\bar{u_i} \geq 0$ by the definition of $\bar{u_i}$.

Since $\overline{\mathscr{H}} \geq 0$ and $\frac{\partial\overline{\mathscr{H}}}{\partial p_i}(u_i+v) \geq 0$, then $\lim_{t\to+\infty}\dot{W}(p_1(t),\ldots,p_n(t))$ exists and must be zero. Suppose the limit is not zero; then, it should be strictly negative, as $-c \leq 0$. But if it is strictly negative, we have that, given $\varepsilon > 0$, there is $T_\varepsilon > 0$, such that $\forall t \geq T_\varepsilon$, $\dot{W}(t) \leq -c+\varepsilon < 0$. But then, $W(t')-W(t) \leq (-c+\varepsilon)(t'-t)$ for all $t', t \geq T_\varepsilon$ and $W(t)$ would not be lower bounded, which is a contradiction.

Proof, Proposition 6.4. For the affine flow, the time-optimal trajectories are given by (7). Taking the gradient of $p_i(t)$ with respect to initial position $p_i(0)$ results in

$$\frac{\partial p_i(t)}{\partial p_i(0)} = e^{At}\,.$$

To connect the above gradient back to the problem of finding $\frac{\partial\zeta_i}{\partial p_i}$, recall that ζ_i is a parameterization of $\partial\mathscr{R}_T(p_{i0})$. Thus points along ζ_i are solutions of the optimal control problem at a particular (fixed) time. The result (15) follows immediately.

Proof, Lemma 6.3. Let $u_i = 0$ for all $i \in \{1,\ldots,n\}$. Then $\dot{\mathscr{H}} = \sum_{i=1}^{n}\frac{\partial\mathscr{H}}{\partial p_i}c$. Suppose an agent i has a region that intersects the boundary of X. Since $u_i = 0$, agent i drifts parallel to the shore. Furthermore, other agents drift at the same rate. Thus, all agents maintain their relative positions and so total area remains constant. Thus $\sum_{i=1}^{n}\frac{\partial\mathscr{H}}{\partial p_i}c = 0$. Now, for u_i as in (14), $\dot{\mathscr{H}} = \sum_{i=1}^{n} v\left\|\frac{\partial\mathscr{H}}{\partial p_i}\right\| \geq 0$.

Proof, Proposition 6.5. We can take the result (17) and take the derivative with respect to initial position p_0 by applying the chain rule. Before launching into the computation, we make a couple observations. The sequence of interface crossing positions $\{\bar{x}_1,\ldots,\bar{x}_q\}$ depends only on the initial heading choice θ_0. In fact, each interface crossing position $\bar{x}_\ell$ depends only on the previous interface crossing $\bar{x}_{\ell-1}$ and the (fixed) choice of direction $\theta_{\ell-1}$ determined by (8). On the other hand, we can express the interface crossing time $\bar{t}_\ell$ as

$$\bar{t}_\ell = \bar{t}_{\ell-1} + \frac{\|\bar{x}_\ell - \bar{x}_{\ell-1}\|}{\|\dot{p}_{\ell-1}\|}\,.$$

Thus, $\bar{t}_\ell$ depends on both the previous interface crossing time and the previous crossing position.

Applying the chain rule to (17), we have

$$\frac{\partial p_T}{\partial p_0} = \frac{\partial\bar{x}_q}{\partial p_0} - \dot{p}_q\frac{\partial\bar{t}_q}{\partial p_0} = \frac{\partial\bar{x}_q}{\partial\bar{x}_{q-1}}\frac{\partial\bar{x}_{q-1}}{\partial p_0} - \dot{p}_q\left[\frac{\partial\bar{t}_q}{\partial\bar{x}_{q-1}}\frac{\partial\bar{x}_{q-1}}{\partial p_0} + \frac{\partial\bar{t}_q}{\partial\bar{t}_{q-1}}\frac{\partial\bar{t}_{q-1}}{\partial p_0}\right].$$

Note that

$$\frac{\partial\bar{x}_q}{\partial\bar{x}_0} = \left(\frac{\partial\bar{x}_q}{\partial\bar{x}_{q-1}}\right)\left(\frac{\partial\bar{x}_{q-1}}{\partial\bar{x}_{q-2}}\right)\cdots\left(\frac{\partial\bar{x}_1}{\partial\bar{x}_0}\right) \triangleq D_q\,.$$

Then

$$\frac{\partial p_T}{\partial p_0} = D_q - \dot{p}_q\left[\frac{\partial\bar{t}_q}{\partial\bar{x}_{q-1}}D_{q-1} + \frac{\partial\bar{t}_{q-1}}{\partial p_0}\right].$$

Repeated application of the chain rule on the last term gives the result.

Proof, Proposition 6.6. Suppose there is a parameterization $\zeta : \mathbb{R} \to \mathbb{R}^2$ of the curve described by $\psi(x) = 0$. Let $\zeta(0)$ correspond to the interface crossing position $\bar{x}$. We wish to find the variation of the crossing position $\bar{x}$ with respect to a change in initial position p_0. For example, in Figure 15, for a horizontal displacement δx, we wish to find

$$\lim_{\|\delta x\| \to 0} \frac{\zeta(\tilde{t}) - \zeta(0)}{\|\delta x\|}, \tag{23}$$

where $\zeta(\tilde{t})$ is the point along the curve ζ that intersects the displaced trajectory. We also wish to find a similar quantity for vertical displacements δy.

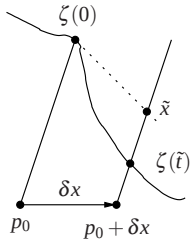

Fig. 15 Diagram for the proof.

Since $\bar{x}$ is constrained to lie on the curve $\zeta(t)$, the derivatives of $\bar{x}$ with respect to the horizontal and vertical variations in initial position must lie along the tangent direction $\zeta'(0)$. One can show that computing

$$\lim_{\|\delta x\| \to 0} \frac{\tilde{x} - \zeta(0)}{\|\delta x\|}, \tag{24}$$

where $\tilde{x}$ is the point along the tangent line from $\zeta(0)$ that intersects the displaced trajectory, is equivalent to computing (23) as $\|\delta x\| \to 0$. The limit (24) is much easier to compute since $\tilde{x}$ can be solved for explicitly.

In other words, we use the linear approximation of $\zeta(t)$ about $\zeta(0) = \bar{x}$ to compute the Jacobian $\frac{\partial \bar{x}}{\partial p_0}$ at the point $\bar{x}$. Let η be the unit normal vector to ζ at $\zeta(0)$. Then, given a constant velocity $\dot{p}$, the intersection point $\tilde{x}$ of a trajectory starting from p_0 to the tangent line through $\zeta(0)$ is given by

$$\tilde{x} = p_0 + \frac{(\zeta(0) - p_0)^\mathsf{T} \eta}{\dot{p}^\mathsf{T} \eta} \dot{p}.$$

The quotient of inner products represents the travel time from p_0 to the tangent line, since the inner products project the travel distance and travel velocity onto the normal direction. Expanding p_0, $\dot{p}$, and η into components and differentiating with respect to horizontal and vertical changes of p_0 yields the final result of (19). In performing the above differentiation, we also differentiate the crossing time with respect to initial position to get (20).

Proof, Proposition 6.7. We assume a non-simple trajectory such as that described in Theorem 5.1. Then, there is a specific point $x^* = \bar{x}_{\ell^*}$ that a trajectory originating from p_0 must pass through to reach points in $\mathscr{U}(p_0)$. This point is *fixed* in space, so the quantity $\frac{\partial \bar{x}_{\ell^*}}{\partial p_0} = 0$. Thus, the expression for the Jacobian (18) becomes (21).

The remaining task is to compute the special term $\frac{\partial \bar{t}_{\ell^*}}{\partial \bar{x}_{\ell^*-1}}$ corresponding to the special crossing point $\bar{x}_{\ell^*}$. For $\ell < \ell^*$, the derivative is given by (20). We begin with

$$\bar{t}_{\ell^*} = \bar{t}_{\ell^*-1} + \frac{\|\bar{x}_{\ell^*} - \bar{x}_{\ell^*-1}\|}{\|\dot{p}_{\ell^*-1}\|}.$$

Then, differentiating with respect to the previous crossing location $\bar{x}_{\ell^*-1}$, we obtain the result (22).